Co/Pt perpendicular antidot arrays with engineered feature size and magnetic properties fabricated on anodic aluminum oxide templates

M. T. Rahman,* N. N. Shams, and C. H. Lai†
Materials Science and Engineering Department, National Tsing Hua University, Hsinchu, Taiwan

J. Fidler and D. Suess
Solid State Physics Department, Vienna University of Technology, Vienna, Austria

(Received 26 March 2009; revised manuscript received 14 December 2009; published 25 January 2010)

Antidot arrays with perpendicular anisotropy have been fabricated by depositing Co/Pt multilayers on the anodic aluminum oxide (AAO) templates prepared on Si wafers. The antidot arrays cover an area of about 10 cm^2. The antidot size (D) and edge-to-edge (w) separation between two adjacent antidots are varied over a wide range from 7 to 46 nm and 14 to 53 nm, respectively. The magnetic properties and magnetization process exhibit strong dependence on the antidot size and separation. The perpendicular coercivity (H_c) increases from 140 Oe (continuous film) with the increase in D and shows a peak at about 1350 Oe for the D of around 30 nm. The H_c starts to decrease for the further increase in D due to the deteriorated perpendicular anisotropy. The magnetization reversal of the antidot arrays with D of 30 nm or less is governed by the strong domain-wall pinning and the switching field shows less sensitivity to the angular variation from the easy axis. The magnetic domain size decreases with increase in D. The evolutions of magnetic properties are ascribed to the pinning effects imposed by the AAO pores. The influence of antidot size on the pinning of domain wall, H_c and magnetization switching characteristics are also investigated by the micromagnetic modeling.

DOI: 10.1103/PhysRevB.81.014418 PACS number(s): 81.07.−b, 75.75.−c, 75.50.Ss, 75.60.Jk

I. INTRODUCTION

Magnetic antidot arrays have been studied extensively for the last decade due to its potential applications for magnetic data storage[1–7] as well as their importance for the understanding of fundamental magnetism in confined geometries, for example, magnetization reversal,[8,9] spin transport,[10] and exchange bias.[11–13] To date, most of the works have been concentrated on the magnetic antidot arrays with in-plane anisotropy. However, the shifting of the magnetic data storage industry from the longitudinal to the perpendicular recording mode indicates that the antidot arrays can be considered as the potential magnetic recording media only when its anisotropy is perpendicularly oriented. Recent theoretical[14,15] and experimental[7,16] demonstrations of a new class of perpendicular magnetic recording media consisting of exchange-coupled grains with nonmagnetic pinning sites, termed as the percolated perpendicular media, have propelled the interest again in the magnetic antidot arrays with perpendicular anisotropy where the pores can serve as the pining sites.[6,7,16] The perpendicular antidot arrays are also interesting from the application point of view in superconductor as flux pining centers.[17,18] As the evolution of magnetic properties in antidot arrays is strictly related to the antidot size and separation, a systematic study with the feature size comparable to the domain-wall (DW) width is a must to gain the full advantages for applications and to understand the underlying mechanism in details. However, such works are significantly lacking due to the challenges of fabrication and characterization of nanostructures in such a small scale. Among the many efforts to fabricate antidot arrays, a simple way is to deposit materials on prepatterned substrates that have been prepared by electron-beam lithography,[1] extreme ultraviolet lithography,[10] or diblock copolymer templates.[19] In particular, anodic aluminum oxide (AAO) templates[3,4,6,12,13] have been proposed for large-area fabrication with potential to achieve sub-10 nm feature size.[4] In contrast to the conventional lithographic top-down methods, the AAO approach offers many advantages, such as high throughput, large-area fabrication at low cost, and small feature size, even smaller than 10 nm.[4,20] In this work, we demonstrate the fabrication of Co/Pt perpendicular antidot arrays covering an area exceeding 10 cm^2 by using AAO/Si templates (AAO prepared on a Si wafer). Unlike the other works[3,12] on the fabrication of antidots by using AAO membranes, the AAO/Si templates offer direct integration of the antidots with the commercially available substrates. We investigate the influence of the antidot size and separation on the magnetic properties and magnetization reversal in details by varying the antidot size from 7 to 46 nm and separation from 14 to 53 nm. Moreover, the underlying mechanisms of the evolution of magnetic properties and magnetic switching characteristics are also investigated by using micromagnetic modeling.

The paper is organized as follows. In Sec. II, we describe the fabrication method of perpendicular magnetic antidot arrays. In Sec. III, the experimental results are interpreted. A comparison between experimental results and simulations is also given. A summary is given in Sec. IV.

II. EXPERIMENTAL PROCEDURE

The fabrication procedure is schematically shown in Figs. 1(a)–1(d). The procedure consists of two main processes: (A) fabrication of AAO/Si templates with different pore diameter (D) and interpore edge-to-edge distance (w) and (B) subsequent deposition of magnetic layer on AAO/Si templates as described below.

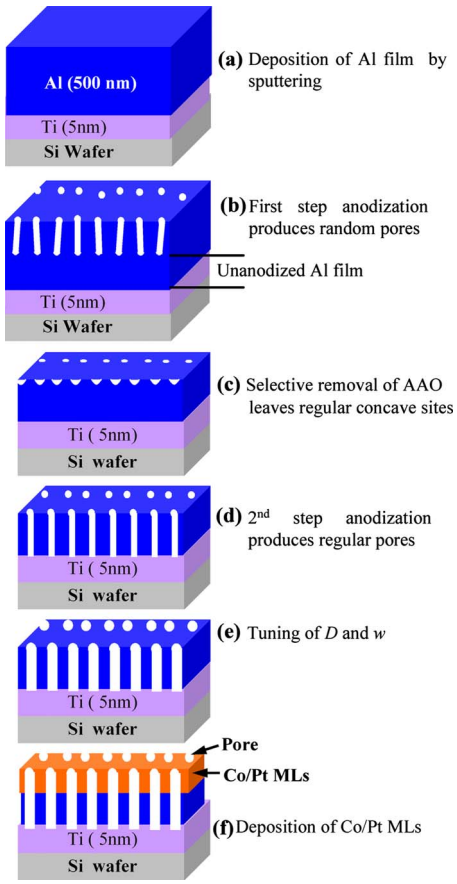

FIG. 1. (Color online) Schematic representation of the fabrication procedure of (Co/Pt) perpendicular antidot arrays.

A. Fabrication of AAO with different pore sizes

At first, a 500 nm Al film with a thin Ti underlayer is deposited by sputtering on a 4 inch Si wafer [Fig. 1(a)]. The sample is then cut into 10 cm^2 pieces. This Al film is anodized at 25 V in 0.3 M H_2SO_4. A two-step anodization process is used to fabricate the ordered alumina nanotemplates on silicon substrates. Typically, the first anodization process is conducted to anodize about 300 nm of the aluminum from the top [Fig. 1(b)]. The first anodized alumina layer is then selectively removed by immersing in 20:80 solution of 2 wt % CrO_3+6 wt % H_3PO_4 for 10 min at 65 °C. The concave texture of the Al surface, formed by the selective removal of the film after the first anodizing step, is used to induce the ordered formation of pores even at the initial stage of anodization in the second step [Fig. 1(c)]. The second anodization step is carried out exactly same as the first anodization step and lasted until the aluminum film is completely converted to alumina [Fig. 1(d)]. The density of the pores is about 4×10^{10} cm^{-2} and the center-to-center distance between two adjacent pores (d) is about 60 nm. The pore widening treatment by chemical wet etching (5 wt % phosphoric acid) is subsequently carried out at 30 °C to control the pore diameter of the AAO [Fig. 1(e)]. The pore diameter is tuned by varying the etching time from 3 to 20 min. The pore diameter is varied from 9 to 48 nm and the edge-to-edge distance between the pores is varied from 51 to 12 nm while the distance between the centers of the neighboring pores is kept constant of about 60 nm [Fig. 1(c)]. The aspect ratio (pore height/diameter) is kept almost the same at about 3 to prevent the deposition of magnetic materials inside the pores at the bottom.[9]

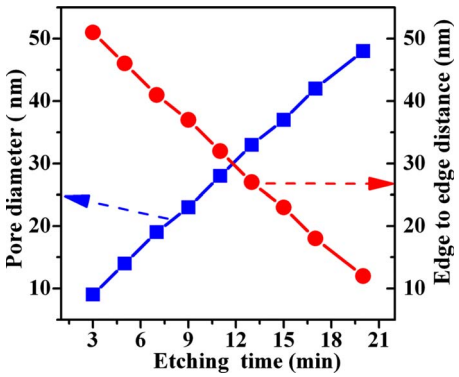

FIG. 2. (Color online) Variations in pore diameter and interpore edge-to-edge distance as a function of etching time.

B. Fabrication and characterization of Co/Pt antidot arrays

$[Co(0.5)/Pt(2)\ nm]_5$ multilayers (MLs) with 7 nm Pt and 3 nm Ta underlayers are then deposited onto the surface of the AAO/Si templates by sputtering at room temperature [Fig. 1(f)]. The base pressure of the sputtering system is below 2×10^{-7} Torr and the working pressure is maintained at 3 mTorr during the deposition. The deposition parameters of the multilayers are chosen to form (111) textured films with a clear layer structure without formation of Co-Pt alloys, revealed from transmission electron microscope (TEM) images.[21] The same magnetic structure is deposited on bare Si wafers for comparison. The surface morphology of the antidot arrays is observed with a field-emission scanning electron microscope (SEM) and TEM. Magnetic properties are measured using a vibrating sample magnetometer. Magnetic domain imaging is performed by a magnetic force microscope (MFM).

III. RESULTS AND DISCUSSION

Figure 2 shows the variations in pore diameter and interpore edge-to-edge separation as a function of the pore widening time. The pore diameter, D increases almost linearly with increasing etching time. As the center-to-center distance between two adjacent pores (d) remains the same at about 60 nm, the edge-to-edge distance ($w=d-D$) decreases automatically with increase in D. Figure 3 shows plane-view SEM image and cross-sectional TEM image of Co/Pt antidot arrays with D and w of 25 and 35 nm, respectively. To check the uniformity of pores over large area, the samples from different parts of the mother sample ($\sim$10 cm^2) used for anodization are observed by SEM. Almost identical features are found all over the mother sample. The dark areas in SEM image correspond to the pores and the bright areas correspond to the magnetic layers supported by the pore walls, that is, AlO_x covered by Co/Pt MLs. The presence of pores is

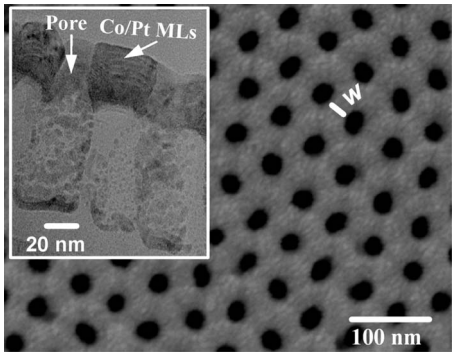

FIG. 3. Plane-view SEM image and TEM cross-sectional image (inset) of Co/Pt antidot array with D and w of 25 and 35 nm, respectively.

clearly visible in all samples. The arrangement of the pores is quite regular and close to being arranged on a hexagonal lattice. TEM cross-sectional imaging is performed to understand the complete topology of the [(Co/Pt)MLs]/AAO/Si structure and is shown in the inset of Fig. 3. The image reveals that the magnetic materials are deposited mainly on the top of the walls and perimeter of the pores, and negligible amounts are at the bottom of the pores. Usually, almost all of the materials remain on top of the walls when the sputtering is performed on such porous substrates with the aspect ratio of the holes larger than 2 (Ref. 9). It is reasonable to assume that most of the materials remain on top of the pore walls in the present work as the aspect ratio is maintained at about 3. As a result, the Co/Pt MLs are percolated by nanopore arrays of AAO. The surface morphology for all samples is nearly the same due to the same aspect ratio of pores. The pore diameter is slightly reduced (or the edge-to-edge distance is increased) after depositing the magnetic film on the AAO template by 2 nm.

The out-of-plane, in-plane, and initial M-H loops for the Co/Pt antidot arrays with different D and w and the reference continuous film deposited under the identical conditions are shown in Figs. 4(b)–4(e) and Fig. 4(a), respectively. The corresponding plane-view SEM images are also shown in Fig. 4. Figure 4(f) shows the schematic representation of the antidot diameter, D, edge-to-edge separation, w, and center-to-center distance d. The SEM images confirm the presence of nanopore arrays in all samples. The w is reduced with increase in D continuously shown in Figs. 4(g)–4(j). As for the magnetic properties, the continuous film exhibits a square M-H loop with very small out-of-plane H_c of only about 140 Oe and negligible H_c in the in-plane direction. As shown in Fig. 4(b), the out-of-plane coercivity, H_c of (Co/Pt) MLs dramatically increases when MLs are deposited on AAO/Si templates and exhibits the maximum value for D at around 30 nm and w of around at 30 nm [Fig. 4(c)]. For the antidot arrays with D of more than 30 nm and w of less than 30 nm, the M-H loops starts to lose the squareness ratio S (the ratio of the remanent magnetization to the saturation magnetization) and perpendicular anisotropy as evidenced by the presence of in-plane M-H loop shown in Figs. 4(d) and 4(e).

To understand the mechanism of coercivity enhancement and magnetization process, we measured the initial magneti-

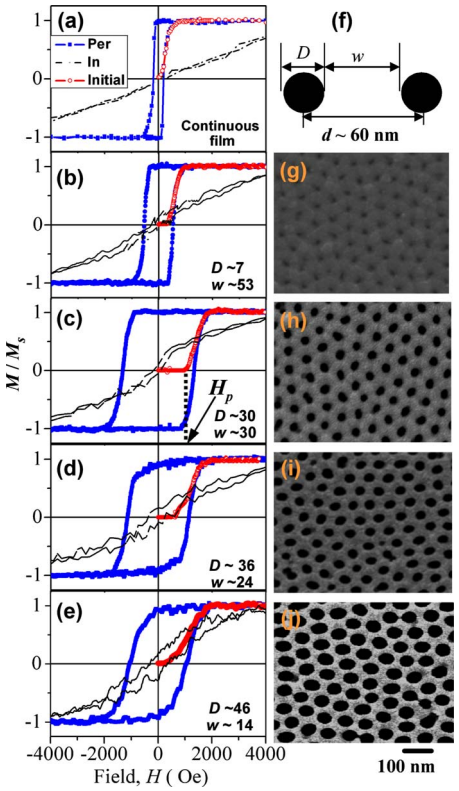

FIG. 4. (Color online) The out-of-plane, in-plane, and initial M-H loops of (a) (Co/Pt) continuous film, [(b)–(e)] (Co/Pt) antidot array, and [(g)–(j)] the corresponding SEM images. (f) Schematic representation of antidot diameter, D, edge-to-edge separation, w, and center-to-center separation, d.

zation curves of all samples as shown in Figs. 4(a)–4(e). The initial magnetization curves are measured after ac demagnetization with a maximum field of 15 kOe. The curves are convex downward with low initial susceptibility, suggesting that the magnetization reversal is mainly controlled by the domain-wall pinning.[16,22] The rise in the initial magnetization curve of (Co/Pt) MLs deposited on the bare Si wafers at a low field indicates easy domain-wall propagation while the magnetization of the (Co/Pt) MLs deposited on AAO/Si templates begins to increase only when the applied field reaches a critical field for the domain walls to become unpinned. This critical field is defined as the pinning field H_p. The variations in H_c and H_p as a function of D and w are plotted in Fig. 5. It is found that H_p and coercive field, H_c are closely related to each other. Both the H_p and H_c of Co/Pt MLs increase sharply for the increase in D from 7 to 30 nm and then start to decrease for further increase in D or decrease in w. The variations in H_p and H_c with pore diameter suggest that the increase in H_c is attributed to the domain-wall pinning[16,23] and the effective pinning becomes stronger with the increase in pore diameter. In order to understand the underlying pinning mechanism, micromagnetic simulations are performed.

The influence of pore diameter and interpore edge-to-edge distance on the H_c and H_p is simulated for the actual geometry. We used the finite-element micromagnetic code FEMME (Ref. 24) to construct an antidot array with the lateral dimen-

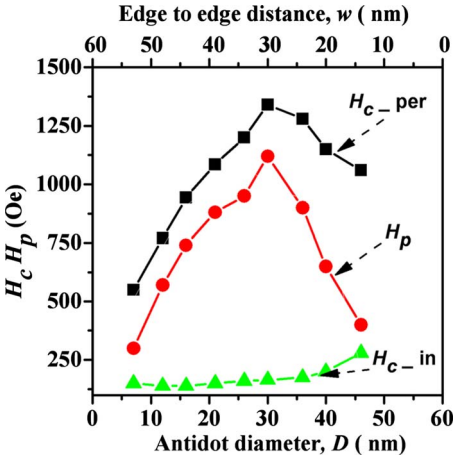

FIG. 5. (Color online) Variations in out-of-plane and in-plane H_c and pinning field, H_p of Co/Pt antidot array as a function of antidot diameter, D and edge-to-edge separation, w.

sions of 500 nm × 500 nm. A finite-element mesh size of 5 nm is used. The diameter of the pores is varied from 14 to 34 nm. The following material parameters are assumed: exchange constant $A=1\times10^{-11}$ J/m, a perpendicular anisotropy $K_1=1\times10^5$ J/m^3, and the magnetic polarization $J_s=\mu_0 M_s=0.44$ T, where μ_0 is the permeability of free space and M_s is the saturation magnetization. In order to be able to calculate the pinning field, we plotted the initial magnetization curve of the constructed antidot geometry for simulation, which consists of two domains as shown in Fig. 6(b)—state A.

Figure 6(a) shows the initial curve of an antidot array with the diameter of $D=14$ and 34 nm, respectively. The external field is applied perpendicular to the film plane. The magnetic states along the initial curves for $D=14$ nm at different magnetic fields show that the domain wall is pinned by the nonmagnetic pores as shown in Fig. 6(b). The pinning field increases with increasing pore diameter as shown in Fig. 6(c). The increase in pinning field with increasing defect diameter D can be attributed to the change in the domain-wall energy (pinning energy), which is saved due to the defects. As discussed in detail in Ref. 25 the pinning energy of a domain wall with a defect in its center can be calculated as

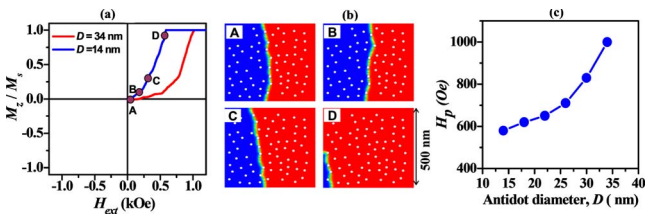

FIG. 6. (Color online). (a) Simulated initial curve of Co/Pt antidot arrays with a diameter of $D=14$ and 34 nm. (b) The z component of the magnetic states along the initial curve for the sample with $D=14$ nm is color coded. Blue and red colors represent magnetization direction pointing down and up, respectively. (c) Variation in the pinning field of antidot arrays with different pore diameters. The pinning fields are extracted from the initial curves when $M_z/M_s=0.2$.

$$E_{pin}\approx 4N\sqrt{AK_1}t\int_{-r}^{r}\tanh\left(\frac{\sqrt{r^2-y^2}}{\delta_0}\right)dy. \quad (1)$$

The variables are as follows: film thickness t, the exchange constant A, the perpendicular anisotropy constant K_1, the radius of the defect $r=D/2$, and the Bloch wall parameter δ_0, which is connected with the domain-wall width according to $\delta_{dw}=\pi\delta_0\pi\sqrt{A/K_1}$. The domain-wall energy is saved by the defect due to the fact that in the defect there is no magnetic material. Hence in this region the domain-wall energy is zero.

In the limit of $\delta_0 \ll D$ we can approximate Eq. (1) by

$$E_{pin}\approx 4N\sqrt{AK_1}tD, \quad (2)$$

which shows the linear increase in pinning energy with the defect diameter D.

The experimentally observed dependence of H_p on the pore diameter, shown in Fig. 5, is good in agreement with the simulation [Fig. 6(c)] for D equal to or less than 30 nm. However, there exists a discrepancy of the experimental dependence of H_p and the simulations for D larger than 30 nm. The decrease in the pinning field in experimental results for pore diameter larger than 30 nm is explained as follows. As shown in Fig. 4, the saturation fields of the hard-axis loops decrease with increasing pore diameter. The hard-axis hysteresis loop of the continuous film is almost perfectly closed and shows the largest saturation field. This indicates a well textured film with high anisotropy. The opening of the hard-axis loop for $D\sim46$ nm indicates a deteriorated perpendicular anisotropy of the film. We assume that the anisotropy near the rim of the pores, instead of being perpendicular, inclines toward the surface.[26] Albrecht *et al.*[27] also observed a variation in anisotropy direction by depositing Co/Pd MLs on spherical nanospheres. This may be a reasonable assumption since the direction of the film deposition on average is perpendicular to the land regions but has a certain angle relative to the pore walls.[28] In our previous study of the effects of pore density on the magnetic properties of the Co/Pt MLs fabricated on AAO/Si templates, we also observed the magnetization tilting around the perimeter of the pores[7,16] but the tilting is more severe in the samples with large diameters in this study due to the large perimeter area.

Hence, we attribute the reduction in H_p and H_c for D of more than 30 nm and w of less than 30 nm to the deteriorated perpendicular anisotropy; in particular, in the region close to the pores. The decrease in perpendicular anisotropy with increasing D can also be realized by comparing the squareness ratio S defined as the ratio of the remanent magnetization to the saturation magnetization. S remains almost unchanged at about 1 up to D equal to 30 nm and starts to decrease for the increase in D, as shown in Figs. 4 and 7. The decreased S was also observed when Co/Pd MLs were deposited on spherical nanospheres.[27] In our simulations, a perfect perpendicular anisotropy with an identical value is assumed for samples with different D without considering the significant variations in the anisotropy axis around the pores, which explains the difference between our simulation and experimental findings for the antidot arrays with D of larger than

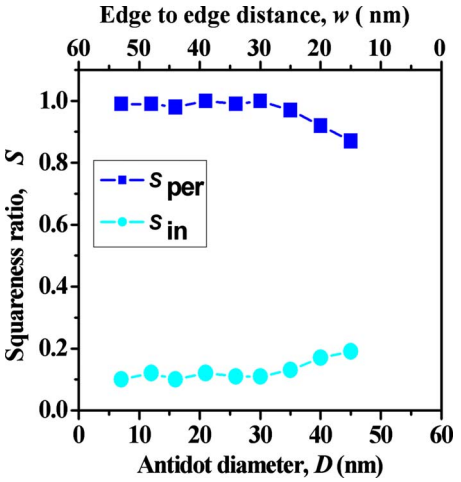

FIG. 7. (Color online) Variations in out-of-plane and in-plane squareness ratio of Co/Pt antidot array as a function of antidot diameter, D and edge-to-edge separation, w.

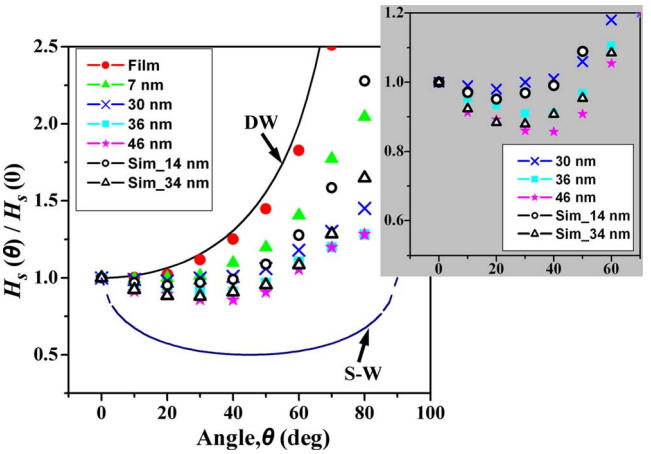

FIG. 8. (Color online) (a) Switching field H_s of (Co/Pt)/Si (continuous) film and Co/Pt antidot array with different D as a function of angle θ between the applied field and the easy axis. The solid lines represent theoretical curves for DW motion and S-W rotation, respectively. The inset is the enlarged figure to clearly show the angular dependence from 0° to 60°.

30 nm. The maximum or a peak in H_p and H_c are observed due to the decrease in H_c caused by the deteriorated perpendicular anisotropy for the D of more than 35 nm.

The magnetization switching characteristics of the continuous film and antidot arrays are investigated experimentally and micromagnetically in more detail by measuring the angular dependence of the switching field, H_s. H_s is defined as the reverse field needed to reduce the remanent magnetization to zero. H_s provides a method to determine magnetization-reversal mechanisms through comparisons with well-known Kondorski[29] and Stoner-Wohlfarth (S-W) models.[30] The Kondorski model[29] describes the magnetization reversal process by the domain-wall motion and the S-W model[30] demonstrates the magnetization reversal process by the rotation mode. Figure 8 is a plot of angular dependence of H_s of Co/Pt MLs deposited on Si and AAO/Si templates with different pore diameters. We first note that the continuous film shows a dramatic increase in H_s as the angle of the applied field is increased away from the easy direction. This is a clear sign that the reversal is dominated by domain-wall motion with negligible pinning. We observe two different kinds of angular dependence of switching fields for the antidot arrays with diameter of 30 nm or less and with diameters more than 30 nm, respectively. The angular dependence of H_s of (Co/Pt) antidot arrays with diameter of 30 nm or less follows neither a pure domain-wall-motion model[32] nor a pure rotation model.[33] Unlike both idealized models, the H_s of antidot arrays with D smaller or equal to 30 nm is quite insensitive to the angle of the applied field when it is smaller than 40°. The angular dependence of the switching field is also confirmed by using the micromagnetic simulations. The simulated angular dependence of antidot arrays with pore diameter of 14 and 34 nm is shown in Fig. 8. The material parameters used in the modeling are kept the same as those used to model the dependence of H_p on antidot diameter as described previously. The micromagnetic modeling confirms that the pores with diameter smaller than 30 nm lead to almost unchanged switching fields for the angles θ between 0° and about 40°. A similar angular dependence was obtained in Co/Pd MLs deposited on nanospheres reported by Albrecht *et al.*[27] In the work of Ref. 27, this kind of switching behavior was ascribed to the variations in anisotropy direction and different film thickness on nanospheres. This explanation can also be valid in our case because the anisotropy direction of Co/Pt MLs around the pore and on the wall may vary.

The slow increase in H_s with the angle and deviation from the DW motion behavior also indicate the increase in the pinning effect[9,16,31] that becomes more profound when the pore diameter is increased up to 30 nm. According to the S-W model as shown in Fig. 8, the H_s drops significantly even for a small-angle variation in the applied field from the easy axis in conventional perpendicular media. This effect contributes to the decrease in signal-to-noise ratio and creates a problem of adjacent track erasure. On the contrary, the unique switching behavior in the fabricated Co/Pt antidot array with D of 30 nm or less provides large tolerance of switching-field distribution, that is, the H_s is less sensitive to the angle of the applied field; therefore, high signal to noise can be expected.[32,33] Furthermore, the constant H_s over large angular deviation may be beneficial for addressing the problem of adjacent track erasure.[33]

For the samples with D of 36 and 46 nm, we observe a qualitatively different behavior in H_s angular dependence because there is now a minimum near 40° as shown clearly in the inset of Fig. 8. For reference, the S-W behavior is shown as a solid line in Fig. 8. Although the angular dependence looks like S-W behavior, we clarifies that the changing angular dependences for different pore diameters is a pure effect of the pinning of domain walls at cylindrical defects, as it can be reproduced well by micromagnetic simulations. The micromagnetic simulation of angular H_s with pore diameter of 34 nm also exhibits a minimum near 30°–40° as shown in Fig. 8.

We also investigate the effect of variations in antidot diameter and edge-to-edge separation on the magnetic domains. Figure 9 shows the MFM images of Co/Pt continuous

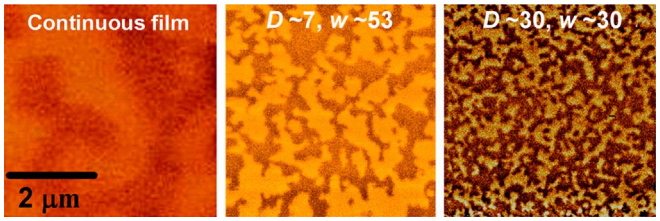

FIG. 9. (Color online) MFM images of (a) (Co/Pt) continuous film and (Co/Pt) antidot array with (b) $D \sim 7$ nm and (c) 30 nm.

film and antidot arrays with different D and w in the ac demagnetized state. The average domain size decreases with increase in D or decrease in w. The average domain size for the continuous film, antidot arrays with D of 7 and 30 nm are 1000, 300, and 100 nm, respectively. It indicates that the decrease in domain size is due to the pinning effect imposed by the pores[4,16] that is good in agreement with the increase in H_c with increasing the pore diameter. This result also suggests that it is possible to tune the domain size by controlling the D and w.

In our earlier study[16] we achieved a 12 times enhancement of perpendicular H_c for the Co/Pt MLs on AAO by optimizing the pore density in antidot arrays with pore diameter of about 12 nm. The squareness ratio was maintained at unity even for the highest density of pores. Comparing to the current results, we suggest that the H_c can be further enhanced with the squareness ratio of unity by optimizing both the density and the size of the pores in magnetic antidots.

IV. CONCLUSION

We introduce a simple and versatile method to control the antidot size, D and separation, w of Co/Pt perpendicular antidot arrays over a wide range from 7 to 46 nm and 14 to 53 nm, respectively. Moreover, we demonstrate that the magnetic properties, magnetization switching mechanism and magnetic domain size can be tuned by engineering the D and w. We achieved one order enhancement of the perpendicular H_c compared to the continuous film that is attributed to the pinning effects of the pores. Furthermore, the experimental results on the dependence of H_p and the angular dependence of H_s are interpreted by micromagnetic simulations. The micromagnetic simulation suggests that the pinning field increases with increasing pore diameter. We attribute the experimentally obtained decrease in the pinning field for pore diameters larger than 30 nm to the lowered perpendicular anisotropy. In particular, it is assumed that the effective anisotropy is decreased near the rim of the pores.

Although the magnetic properties are shown for Co/Pt MLs, the approach is versatile to any magnetic material to engineer the optimum pinning effect in pinning-type magnets, which may be applied for future high-density recording media.

ACKNOWLEDGMENTS

This work is supported by the National Science Council and Ministry of Economic Affairs of Republic of China under Grants No. NSC 95-2221-E-007-063-MY2 and No. 95-EC-17-A-08-S1-0006, respectively. The financial support of the FWF project P20306 is also acknowledged.

*Present address: Electrical and Computer Engineering Department, The Center for Micromagnetics and Information Technologies (MINT), University of Minnesota, Minneapolis, MN 55455, USA; rahma070@umn.edu

†chlai@mx.nthu.edu.tw

[1] R. P. Cowburn, A. O. Adeyeye, and J. A. C. Bland, Appl. Phys. Lett. **70**, 2309 (1997).

[2] A. Y. Toporov, R. M. Langford, and A. K. Petford-Long, Appl. Phys. Lett. **77**, 3063 (2000).

[3] Z. L. Xiao, C. Y. Han, U. Welp, H. H. Wang, V. K. Vlasko-Vlasko, W. K. Kwok, D. J. Millar, J. M. Hiller, R. E. Cook, G. A. Willing, and G. W. Crabtree, Appl. Phys. Lett. **81**, 2869 (2002).

[4] M. T. Rahman, N. N. Shams, and C. H. Lai, Nanotechnology **19**, 325302 (2008).

[5] For a review see J. I. Martín, J. Nogués, K. Liu, J. L. Vicent, and I. K. Schuller, J. Magn. Magn. Mater. **256**, 449 (2003), and references therein.

[6] M. T. Rahman, X. Liu, and A. Morisako, J. Appl. Phys. **99**, 08G904 (2006).

[7] M. T. Rahman, C. H. Lai, D. Vokoun, and N. N. Shams, IEEE Trans. Magn. **43**, 2133 (2007).

[8] L. J. Heyderman, F. Nolting, D. Backes, S. Czekaj, L. Lopez-Diaz, M. Kläui, U. Rüdiger, C. A. F. Vaz, J. A. C. Bland, R. J. Matelon, U. G. Volkmann, and P. Fischer, Phys. Rev. B **73**, 214429 (2006).

[9] M. T. Rahman, R. K. Dumas, N. Eibagi, N. N. Shams, Y. C. Wu, K. Liu, and C. H. Lai, Appl. Phys. Lett. **94**, 042507 (2009).

[10] C. C. Wang, A. O. Adeyeye, and N. Singh, Appl. Phys. Lett. **88**, 222506 (2006).

[11] M. T. Rahman, N. N. Shams, D. S. Wang, and C. H. Lai, Appl. Phys. Lett. **94**, 082503 (2009).

[12] K. Liu, S. M. Baker, M. Tuominen, T. P. Russell, and I. K. Schuller, Phys. Rev. B **63**, 060403(R) (2001).

[13] N. N. Shams, M. T. Rahman, and C. H. Lai, J. Appl. Phys. **105**, 07D722, (2009).

[14] J. Zhu and Y. Tang, J. Appl. Phys. **99**, 08Q903 (2006).

[15] D. Suess, J. Fidler, K. Porath, T. Schrefl, and D. Weller, J. Appl. Phys. **99**, 08G905 (2006).

[16] M. T. Rahman, N. N. Shams, Y. C. Wu, C. H. Lai, and D. Suess, Appl. Phys. Lett. **91**, 132505 (2007).

[17] M. Lange, M. J. Van Bael, V. V. Moshchalkov, and Y. Bruynseraede, J. Magn. Magn. Mater. **240**, 595 (2002).

[18] E. T. Filby, A. A. Zhukov, P. A. J. De Groot, M. A. Ghanem, P. N. Bartlett, and V. V. Metlushko, Appl. Phys. Lett. **89**, 092503 (2006).

[19] V. P. Chuang, W. Jung, C. A. Ross, J. Y. Cheng, O. H. Park, and H. C. Kim, J. Appl. Phys. **103**, 074307 (2008).

[20] Y. Matsui, K. Nishio, and H. Masuda, Small **2**, 522 (2006).
[21] M. S. Lin and C. H Lai, J. Appl. Phys. **101**, 09D121 (2007).
[22] T. Suzuki, N. Honda, and K. Ouchi, J. Appl. Phys. **85**, 4301 (1999).
[23] H. R. Hilzinger and H. Kronmüller, J. Magn. Magn. Mater. **2**, 11 (1976).
[24] D. Suess, V. Tsiantos, T. Schrefl, J. Fidler, W. Scholz, H. Forster, R. Dittrich, and J. J. Miles, J. Magn. Magn. Mater. **248**, 298 (2002).
[25] D. Punz, D. Suess, and J. Fidler (unpublished).
[26] J. A. Barnard, N. Fujiwara, V. R. Inturi, J. D. Jarratt, T. W. Scharf, and J. L. Weston, Appl. Phys. Lett. **69**, 2758 (1996).
[27] M. Albrecht, G. Hu, I. L. Guhr, T. C. Ulbrich, J. Boneberg, P. Leiderer, and G. Schatz, Nature Mater. **4**, 203 (2005).
[28] Y. C. Hsieh and M. Mansuripur, J. Appl. Phys. **78**, 380 (1995).
[29] E. Kondorski, Phys. Z. Sowjetunion **11**, 597 (1937).
[30] E. C. Stoner and E. P. Wohlfarth, Philos. Trans. R. Soc. London **240**, 599 (1948).
[31] I. Panagiotopoulos, M. Gjoka, and D. J. Niarchos, J. Magn. Magn. Mater. **279**, 389 (2004).
[32] R. H. Victora and X. Shen, IEEE Trans. Magn. **41**, 2828 (2005).
[33] D. Suess, T. Schrefl, R. Dittrich, R. Kirschner, F. Dorfbauer, and J. Fidler, J. Magn. Magn. Mater. **290-291**, 551 (2005).